Volume 1 | Number 1 | Jan 2013 | Pages 1–100

RSC Advances

www.rsc.org/advances

ROYAL SOCIETY OF CHEMISTRY

www.rsc.org/advances

RSC Advances

Dynamic Article Links ▶

Communication

Water intrusion-extrusion experiments in ZIF-8: Impacts of the shape and particle size on the energetic performances

Ismail Khay,[a] Gérald Chaplais,*[a] Habiba Nouali,[a] Claire Marichal[a] and Joël Patarin*[a]

The energetic performances of "ZIF-8–water" systems were evaluated using intrusion-extrusion of water under high pressure. Depending on the shape (spherical, cubic or rhombic dodecahedron) as well as the crystallite size
10 **(nanometric or micrometric scale), the energetic behaviour of the "ZIF-8–water" system can be modified.**

Metal-Organic Frameworks (MOFs) are the latest class of crystallized porous solids. This new class of organic–inorganic hybrid compounds are involved in many potential applications
15 such as capture, storage and separation of gas,[1-4] luminescence,[5-7] magnetism,[8] heterogeneous catalysis,[9-11] mechanical aspects[12] and drug delivery.[13, 14] Recently, this family of porous materials and more particularly the Zeolitic Imidazolate Frameworks (ZIFs) have been studied by our group for applications in the
20 field of energetic, by using intrusion–extrusion of water and aqueous electrolyte solutions under high pressure.[15-17] The phenomenon is based on the following principle: in hydrophobic porous materials, the water condensation (intrusion) is obtained by applying a high hydraulic pressure.[18] Thus, the supplied
25 mechanical energy during the compression step is converted to interfacial energy. By reducing the pressure, the system is able to induce an expulsion of the liquid out of the cavities of the material (extrusion). Depending on various physicochemical parameters, such as the material structure, the pore size, the
30 porous system (cages or channels), and dimensionality of the channels,[19] the system is able to restore, dissipate, or absorb the supplied mechanical energy. Consequently, spring, bumper or shock-absorber behaviour can be observed.

The ZIF topologies mimic those of aluminosilicate zeolites with
35 transition metals (zinc, cobalt, cadmium, copper, etc.) as nodes, linked by imidazolate or benzimidazolate ligands.[20-24] Among the ZIF-type materials, the most studied solid is ZIF-8 which displays a high hydrophobic character and water stability,[20, 25, 26] even if it still remains a matter of debate in the literature.[27, 28] Moreover, it
40 is worth noting that it is one of the few commercially available MOFs and known as Basolite Z1200 because of its great potential. ZIF-8 (Zn(MeIm)$_2$, where HMeIm = 2-methylimidazole) presents a Sodalite (SOD) framework topology (cubic symmetry, space group $I\bar{4}3m$) with a cage diameter of
45 11.6 Å and a 3.3 - 3.4 Å cage aperture delimited by 6 and 4 membered-rings.[20, 23, 26] It is worthy to note that the pore aperture is able to evolve thanks to the "gate opening" effect occurring under external stimuli[29, 30] and enabling the accommodation of

large molecules such as, for instance, para-xylene.[31] In addition,
50 this material possesses a high microporous volume of around 0.6 cm^3 g^{-1}.[26, 32, 33] We have recently shown that the ''ZIF-8–water'' system acts as a shock-absorber under high pressure water intrusion with a stored energy of 13.3 J g^{-1} and the phenomenon is reproducible over several cycles.[15]
55 The energetic performances, in particular, the intrusion pressure depends also on the nature of the non-wetting liquid. Thus, the addition of salts such as KCl, NaCl, LiCl into the "ZIF-8–water" system strongly increases the energetic performances and a transformation of the system behavior from shock-absorber to
60 bumper was observed.[16] Recently, the effect of the crystal size (from nanometer to micrometer scales) of purely siliceous MFI zeolites on the intrusion pressure was investigated, by using high-pressure intrusion-extrusion experiments and no real influence has been observed.[34] The decrease of the energetic performances
65 for the nanosized crystals was explained by the presence of non-crystalline silica regions and therefore a decrease of the porosity available for intrusion.

The influences of the shape and size of the MOF crystals on the energetic performances remain unexplored to date whereas they
70 play a crucial role in adsorption or separation.[35-37] In this way, this work focuses on the synthesis of nanometer (N)- and micrometer (M)-sized ZIF-8 samples with a spherical (S), cubic (C), cubic with truncated edges (CTE), and rhombic dodecahedron (RD) shape, as well as on the assessment of the
75 energetic performances of the corresponding "ZIF-8–water" systems by using intrusion-extrusion of water under high pressure. The samples were synthesized according to the literature (see Experimental Section in Supporting Information†).[38-41] Furthermore, they were fully characterized
80 before and after water intrusion-extrusion experiments by powder X-ray diffraction, N$_2$ adsorption-desorption measurements at 77 K, thermogravimetric analysis (TG) and Scanning Electron Microscopy (SEM).

85

90

RSC Advances Accepted Manuscript
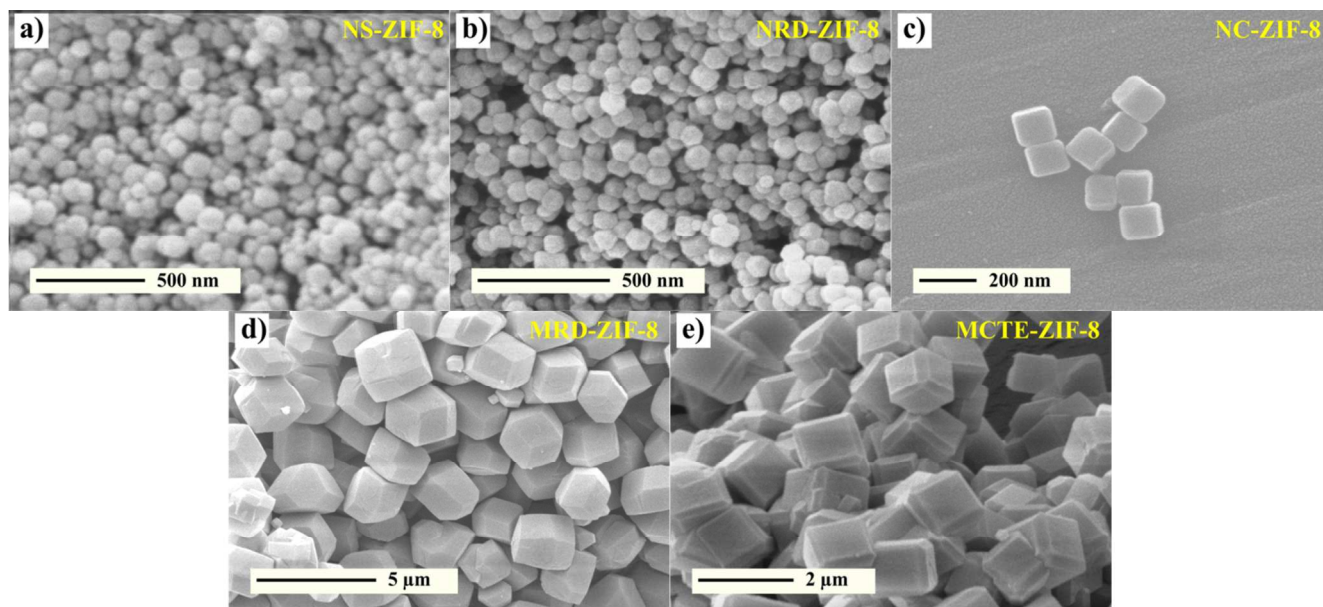
Fig. 1 SEM micrographs of the (a) nanometer-sized spherical crystals (NS-ZIF-8), (b) nanometer-sized rhombic dodecahedron crystals (NRD-ZIF-8), (c) nanometer-sized cubic crystals (NC-ZIF-8), (d) micrometer-sized rhombic dodecahedron crystals (MRD-ZIF-8) and (e) micrometer-sized cubic crystals with truncated edges (MCTE-ZIF-8).

Table 1 Crystal shapes and sizes of the various ZIF-8 samples.

Sample name	Description	Shape[a]	Average size
NS-ZIF-8	Nanometer-sized Spheres		120 nm
NRD-ZIF-8	Nanometer-sized Rhombic Dodecahedra		90 nm
NC-ZIF-8	Nanometer-sized Cubes		130 nm
MRD-ZIF-8	Micrometer-sized Rhombic Dodecahedra		3.2 μm
MCTE-ZIF-8	Micrometer-sized Cubes with Truncated Edges		1.3 μm

[a] Crystal shapes have been designed from VESTA 3 software.[42] Yellow and red facets represent the (110) and (100) planes respectively.

The shape and the crystal size of the prepared ZIF-8 samples were determined from the SEM micrographs (Figure 1). The ZIF-8 samples display either spherical, rhombic dodecahedron or cubic shapes with a crystal size ranging from 90 nm to 3.2 μm (Table 1 and Figure S1 in the Supporting Information†).

Those different samples offering various shapes in both nano- and micrometer domains were assessed by water intrusion-extrusion experiments using high pressure. The pressure-volume diagrams of the "ZIF-8–water" systems are illustrated in Figure 2 and the corresponding characteristic data are reported in Table 2.
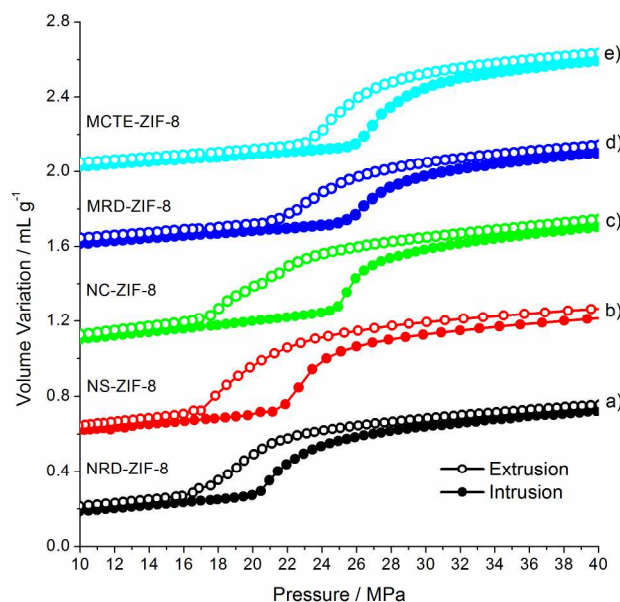
Fig. 2 Pressure-volume diagrams of the first intrusion-extrusion cycle of the (a) "NRD-ZIF-8–water", (b) "NS-ZIF-8–water", (c) "NC-ZIF-8–water", (d) "MRD-ZIF-8–water" and (e) "MCTE-ZIF-8–water" systems. For a better visibility, the diagrams are shifted along the Y-axis.

For each system, three intrusion-extrusion cycles were performed and reproducible results were obtained. For clarity, only the first intrusion-extrusion cycles, in the 10 - 40 MPa range, are reported. Between 0 and 10 MPa, the diagrams (not shown) did not show any phenomenon excepted, as already mentioned in our previous works,[15] a volume variation corresponding to the compressibility of the particles bed and the water intrusion in the interparticular porosity, for a pressure lower than 0.3 MPa.

RSC Advances

Communication

Table 2 Characteristics of the samples: Start intrusion ($P_{1\,int}$), Intrusion (P_{int}), Extrusion (P_{ext}) and Final extrusion ($P_{2\,ext}$) Pressures, Intruded (V_{int}) and Extruded (V_{ext}) Volumes, Stored (E_s) and Restored (E_r) Energies.

	Sample	$P_{1\,int}$[a] (MPa)	P_{int}[a] (MPa)	V_{int}[a] (mL g⁻¹)	P_{ext}[a] (MPa)	$P_{2\,ext}$[a] (MPa)	V_{ext}[a] (mL g⁻¹)	E_s[b] (J g⁻¹)	E_r[b] (J g⁻¹)	Energy yield[c] (%)
Nanometer-sized ZIF-8	NRD-ZIF-8	19.9	~21	0.41	~19	15.9	0.41	8.8	8.0	90.9
	NS-ZIF-8	21.9	~23	0.48	~20	15.9	0.48	11.3	9.5	84.6
	NC-ZIF-8	24.9	~26	0.42	~21	16.5	0.42	10.9	8.8	80.7
Micrometer-sized ZIF-8	MRD-ZIF-8	25.4	~27	0.40	~24	20.6	0.40	10.8	9.8	90.7
	MCTE-ZIF-8	25.9	~28	0.45	~26	22.1	0.45	12.5	11.6	93.3

[a] Determined from the water pressure-volume diagrams. [b] The stored energy (E_s) and restored energy (E_r) values correspond to the area located between the relevant curve of intrusion or extrusion, respectively, and the volume axis (see Figure 1), and are given by: $E = \int_{V_0}^{V_f} P\,dV$, where V_0 is the initial
5 volume and V_f is the final volume. [c] Energy yield = E_r / E_s x 100.

All "ZIF-8–water" systems act as a shock-absorber. For all of them, the intruded volume, close to 0.5 mL g⁻¹, is lower than the one obtained from N_2 adsorption-desorption isotherms (Table S1, † *i.e.*, from 0.64 to 0.66 cm³ g⁻¹). Such a difference was already
10 observed for numerous "zeosil–water" systems and in our previous works concerning ZIF-8.[15, 16] It was explained by a bulk water density lower than 1.[43] In our case the density of bulk water is close to 0.8.

Contrary to what was observed by Humplik *et al.* on zeolite
15 material,[34] the start intrusion pressure ($P_{1\,int}$) increases from nano- to micrometer ZIF-8 crystal size. This latter is equal to 19.9, 21.9, 24.9, 25.4, and 25.9 MPa for the "NRD-ZIF-8–water", "NS-ZIF-8–water", "NC-ZIF-8–water", "MRD-ZIF-8–water" and "MCTE-ZIF-8–water" systems, respectively (Table 2). Furthermore, the
20 intrusion pressure (P_{int}) increases with the particle size and for each sample, the intrusion volume (V_{int}) and extrusion volume (V_{ext}) are similar. Consequently, an increase of the stored energy (E_s) is observed in the case of the ''MCTE-ZIF-8–water'' system (~ 12.5 J g⁻¹) compared to the ''NRD-ZIF-8–water'' system (~
25 8.8 J g⁻¹) corresponding to an energetic gain of 42 %.

Similar trend was also noticed on both the final extrusion pressure ($P_{2\,ext}$), that increases from 15.9 - 16.5 MPa (for NRD-ZIF-8, NS-ZIF-8 and NC-ZIF-8) to 20.6 - 22.1 MPa (for MRD-ZIF-8, and MCTE-ZIF-8) and the extrusion pressure (P_{ext}) (Table
30 2). This might be explained by the presence of a larger number of local defects in the ZIF-8 nanoparticles compared to the ZIF-8 microparticles. Indeed, the framework defects probably contribute to maintain water into the porosity at lower pressure.

Besides the effect of the crystal size on the intrusion-extrusion of
35 water, an effect due to the particle shape is also observed. Indeed, in each group of size (nanometer or micrometer), the sample with the rhombic dodecahedron shape exhibits a lower starting intrusion pressure ($P_{1\,int}$) (and also a lower intrusion pressure P_{int}) than those of the cubic and cubic with truncated edges shaped
40 ZIF-8 samples (Table 2). This might be related to the fact that rhombic dodecahedron shaped particles (NRD- and MRD-ZIF-8 samples) displays only the {110} facets whereas the cubic and

cubic with truncated edges shaped ones (NC- and MCTE-ZIF-8 samples, respectively) presents only or mainly the {100} facets.[44]
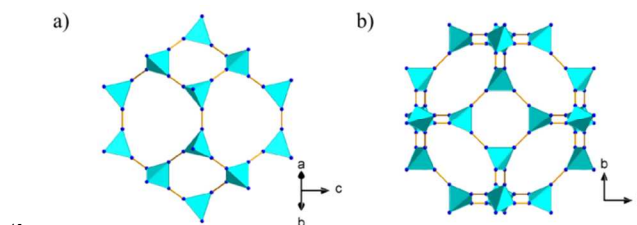
45
Fig. 3 Polyhedral representations of the sodalite cage of ZIF-8 towards (a) the (110) plane related to rhombic dodecahedron shape and (b) the (100) plane related to cubic shape.

Figure 3 represents two projections of the ZIF-8 structure towards
50 (110) and (100) planes, respectively. In the latter case, the cage aperture delimited by 4-membered-rings is directly exposed, whereas in the former case, 4- and 6-membered-rings cage apertures are exposed in a similar manner. By assuming that the water intrusion occurs preferentially through the 6-membred-
55 rings, it is disadvantaged for cubic or cubic with truncated edges shapes (only or mainly {100} facets). Regarding the intermediate values measured for the NS-ZIF-8 sample (inside the nanometer sized group), they might be interpreted by a homogenous random distribution of the {100} and {110} facets on the surface of the
60 crystallites.

In order to assess the stability of the ZIF-8 framework upon high pressure intrusion-extrusion of water, all samples were characterized by XRD, SEM and N_2 adsorption-desorption measurements at 77 K. The XRD patterns of the ZIF-8 samples
65 before and after water intrusion-extrusion experiments are reported in Figure S2.† After three water intrusion-extrusion cycles, no significant changes are observed, which means that, at a long range order, the ZIF-8 structure is preserved. These results confirm the high stability of the crystalline structure after the
70 water intrusion-extrusion process. The morphology of the crystals of the ZIF-8 samples was examined by scanning electron microscopy (Figure S3†). Before and after water intrusion-

extrusion experiments, the ZIF-8 samples display a similar morphology. The N_2 adsorption-desorption isotherms of the non-intruded and intruded samples are shown in Figure S4.† In all cases, the isotherms are mainly of type I featuring microporous materials. After three water intrusion-extrusion cycles, a negligible decrease of the microporous volume (V_μ), the BET surface area (S_{BET}) and Langmuir surface (S_L) area is observed. The corresponding V_μ, S_{BET} and S_L values are reported in Table S1.† It is worth noting that for the NRD-ZIF-8, NS-ZIF-8 and NC-ZIF-8 samples, an increase of the adsorbed volume revealing the presence of capillary condensation was observed for $p/p°$ above 0.9. The latter corresponds to the interparticular porosity between the nanocrystals. The experimental results issued from the thermogravimetric (TG) analysis of the ZIF-8 samples before and after intrusion-extrusion experiments are depicted in Figure S5.† In all cases, the curves of the non-intruded and the intruded-extruded samples are similar. The total weight loss observed in the temperature range 250-600 °C (64.1 wt %, 63.5 wt %, 64.7 wt %, 64.3 wt % and 64.1 wt % for the NRD-ZIF-8, NS-ZIF-8, NC-ZIF-8, MRD-ZIF-8 and MCTE-ZIF-8 samples, respectively) corresponds to the collapse of the ZIF-8 structure which leads to the formation of ZnO. It is in good agreement with the calculated value (64.2 wt %). Besides, it is worth noting that for all samples no weight loss was observed between 30 and 250 °C confirming the hydrophobic character of the ZIF-8 and ruling out the presence of water in the porosity even after three water intrusion-extrusion cycles.

Conclusions

In summary, the energetic performances of "ZIF-8–water" systems were evaluated using intrusion-extrusion of water under high pressure. The intrusion pressure increases from nano- to micrometer ZIF-8 crystal size. Depending on the shape of the crystallites, that is, cubic or rhombic dodecahedron, the energetic performances of the "ZIF-8–water" system can be tuned. The highest values for the intrusion pressure and thereby the stored energy are found for cubic shaped crystallites. All systems, with values of the energy yield varying from 80 to 93%, act as a shock-absorber even as a fairly good shock-absorber for NC-ZIF-8 since the hysteresis is more pronounced in this case. All physico-chemical characterizations, before and after three intrusion-extrusion cycles, clearly demonstrate the high stability of the ZIF-8 framework during the water intrusion-extrusion process under high pressure.

Acknowledgments

Notes and references

^{a} Université de Strasbourg, Université de Haute Alsace, Equipe Matériaux à Porosité Contrôlée (MPC), Institut de Science des Matériaux de Mulhouse (IS2M), UMR CNRS 7361, ENSCMu, 3 bis rue Alfred Werner, F-68093 Mulhouse Cedex, France. Tel: +33 3 89 33 68 87; E-mail: gerald.chaplais@uha.fr; Tel: +33 3 89 33 68 80; E-mail: joel.patarin@uha.fr

† Electronic Supplementary Information (ESI) available: Details of the synthesis procedures of ZIF-8 materials, particle size distribution, X-ray diffraction patterns, SEM pictures, N_2 adsorption-desorption isotherms and curves of thermogravimetric analyses are provided. See DOI: 10.1039/b000000x/

1   K. Sumida, D. L. Rogow, J. A. Mason, T. M. McDonald, E. D. Bloch, Z. R. Herm, T.-H. Bae and J. R. Long, *Chem. Rev.*, 2011, **112**, 724.

2   M. P. Suh, H. J. Park, T. K. Prasad and D.-W. Lim, *Chem. Rev.*, 2011, **112**, 782.

3   L. J. Murray, M. Dinca and J. R. Long, *Chem. Soc. Rev.*, 2009, **38**, 1294.

4   J.-R. Li, J. Sculley and H.-C. Zhou, *Chem. Rev.*, 2011, **112**, 869.

5   M. D. Allendorf, C. A. Bauer, R. K. Bhakta and R. J. T. Houk, *Chem. Soc. Rev.*, 2009, **38**, 1330.

6   Y. Cui, Y. Yue, G. Qian and B. Chen, *Chem. Rev.*, 2011, **112**, 1126.

7   L. E. Kreno, K. Leong, O. K. Farha, M. Allendorf, R. P. Van Duyne and J. T. Hupp, *Chem. Rev.*, 2011, **112**, 1105.

8   M. Kurmoo, *Chem. Soc. Rev.*, 2009, **38**, 1353.

9   J. Lee, O. K. Farha, J. Roberts, K. A. Scheidt, S. T. Nguyen and J. T. Hupp, *Chem. Soc. Rev.*, 2009, **38**, 1450.

10 L. Ma, C. Abney and W. Lin, *Chem. Soc. Rev.*, 2009, **38**, 1248.

11 M. Yoon, R. Srirambalaji and K. Kim, *Chem. Rev.*, 2011, **112**, 1196.

12 W. Li, S. Henke and A. K. Cheetham, *APL Mater.*, 2014, **2**, 123902.

13 P. Horcajada, T. Chalati, C. Serre, B. Gillet, C. Sebrie, T. Baati, J. F. Eubank, D. Heurtaux, P. Clayette, C. Kreuz, J. S. Chang, Y. K. Hwang, V. Marsaud, P. N. Bories, L. Cynober, S. Gil, G. Ferey, P. Couvreur and R. Gref, *Nat. Mater.*, 2010, **9**, 172.

14 P. Horcajada, R. Gref, T. Baati, P. K. Allan, G. Maurin, P. Couvreur, G. Férey, R. E. Morris and C. Serre, *Chem. Rev.*, 2012, **112**, 1232.

15 G. Ortiz, H. Nouali, C. Marichal, G. Chaplais and J. Patarin, *Phys. Chem. Chem. Phys.*, 2013, **15**, 4888.

16 G. Ortiz, H. Nouali, C. Marichal, G. Chaplais and J. Patarin, *J. Phys. Chem. C*, 2014, **118**, 7321.

17 G. Ortiz, H. Nouali, C. Marichal, G. Chaplais and J. Patarin, *J. Phys. Chem. C*, 2014, **118**, 21316.

18 V. Eroshenko, R. C. Regis, M. Soulard and J. Patarin, *J. Am. Chem. Soc.*, 2001, **123**, 8129.

19 L. Tzanis, M. Trzpit, M. Soulard and J. Patarin, *J. Phys. Chem. C*, 2012, **116**, 20389.

20 K. S. Park, Z. Ni, A. P. Côte, J. Y. Choi, R. D. Huang, F. J. Uribe-Romo, H. K. Chae, M. O'Keeffe and O. M. Yaghi, *Proc. Natl. Acad. Sci. USA*, 2006, **103**, 10186.

21 H. Hayashi, A. P. Cote, H. Furukawa, M. O'Keeffe and O. M. Yaghi, *Nat. Mater.*, 2007, **6**, 501.

22 R. Banerjee, A. Phan, B. Wang, C. Knobler, H. Furukawa, M. O'Keeffe and O. M. Yaghi, *Science*, 2008, **319**, 939.

23 A. Phan, C. J. Doonan, F. J. Uribe-Romo, C. B. Knobler, M. O'Keeffe and O. M. Yaghi, *Acc. Chem. Res.*, 2010, **43**, 58.

24 Y.-Q. Tian, S.-Y. Yao, D. Gu, K.-H. Cui, D.-W. Guo, G. Zhang, Z.-X. Chen and D.-Y. Zhao, *Chem. - Eur. J.*, 2010, **16**, 1137.

25 P. Küsgens, M. Rose, I. Senkovska, H. Fröde, A. Henschel, S. Siegle and S. Kaskel, *Microporous Mesoporous Mater.*, 2009, **120**, 325.

26 J. C. Saint Remi, T. Rémy, V. Van Hunskerken, S. van de Perre, T. Duerinck, M. Maes, D. De Vos, E. Gobechiya, C. E. A. Kirschhock, G. V. Baron and J. F. M. Denayer, *ChemSusChem*, 2011, **4**, 1074.

27 X. Liu, Y. Li, Y. Ban, Y. Peng, H. Jin, H. Bux, L. Xu, J. Caro and W. Yang, *Chem. Commun.*, 2013, **49**, 9140.

28 P. Cheng and Y. H. Hu, *J. Phys. Chem. C*, 2014, **118**, 21866.

29 S. A. Moggach, T. D. Bennett and A. K. Cheetham, *Angew. Chem., Int. Ed.*, 2009, **48**, 7087.

30 B. R. Pimentel, A. Parulkar, E.-K. Zhou, N. A. Brunelli and R. P. Lively, *ChemSusChem*, 2014, **7**, 3202.

31 D. Peralta, G. Chaplais, J.-L. Paillaud, A. Simon-Masseron, K. Barthelet and G. D. Pirngruber, *Microporous Mesoporous Mater.*, 2013, **173**, 1.

32 A. Ö. Yazaydin, R. Q. Snurr, T.-H. Park, K. Koh, J. Liu, M. D. LeVan, A. I. Benin, P. Jakubczak, M. Lanuza, D. B. Galloway, J. J. Low and R. R. Willis, *J. Am. Chem. Soc.*, 2009, **131**, 18198.

33 J. Pérez-Pellitero, H. Amrouche, Flor R. Siperstein, G. Pirngruber, C. Nieto-Draghi, G. Chaplais, A. Simon-Masseron, D. Bazer-Bachi, D. Peralta and N. Bats, *Chem. - Eur. J.*, 2010, **16**, 1560.

34 T. Humplik, R. Raj, S. C. Maroo, T. Laoui and E. N. Wang, *Microporous Mesoporous Mater.*, 2014, **190**, 84.

35 G. Kumari, K. Jayaramulu, T. K. Maji and C. Narayana, *J. Phys. Chem. A*, 2013, **117**, 11006.

36 C. Zhang, J. A. Gee, D. S. Sholl and R. P. Lively, *J. Phys. Chem. C*, 2014, **118**, 20727.

37 N. A. H. M. Nordin, A. F. Ismail, A. Mustafa, R. S. Murali and T. Matsuura, *RSC Adv.*, 2014, **4**, 52530.

38 S. Tanaka, K. Kida, M. Okita, Y. Ito and Y. Miyake, *Chem. Lett.*, 2012, **41**, 1337.

39 Z. Li and H. C. Zeng, *Chem. Mater.*, 2013, **25**, 1761.

40 Y. Pan, D. Heryadi, F. Zhou, L. Zhao, G. Lestari, H. Su and Z. Lai, *CrystEngComm*, 2011, **13**, 6937.

41 M. He, J. Yao, Q. Liu, K. Wang, F. Chen and H. Wang, *Microporous Mesoporous Mater.*, 2014, **184**, 55.

42 K. Momma and F. Izumi, *J. Appl. Crystallogr.*, 2011, **44**, 1272.

43 N. Desbiens, I. Demachy, A. H. Fuchs, H. Kirsch-Rodeschini, M. Soulard and J. Patarin, *Angew. Chem., Int. Ed.*, 2005, **44**, 5310.

44 J. Cravillon, C. A. Schroder, H. Bux, A. Rothkirch, J. Caro and M. Wiebcke, *CrystEngComm*, 2012, **14**, 492.